Characterizing the Transcriptome of Turkey Hemorrhagic Enteritis Virus

Running Title: Novel Insights into Turkey Hemorrhagic Enteritis Virus Transcriptome

Abraham Quaye[1*], Brett Pickett[*], Joel S. Griffitts[*], Bradford K. Berges[*], Brian D. Poole[†*]

[*]Department of Microbiology and Molecular Biology, Brigham Young University

[1]First-author

[†] Corresponding Author

Corresponding Author Information

brian_poole@byu.edu

Department of Microbiology and Molecular Biology,

4007 Life Sciences Building (LSB),

Brigham Young University,

Provo, Utah

ABSTRACT

Background: Hemorrhagic enteritis (HE) is a disease affecting 6-12-week-old turkeys characterized by *immunosuppression (IS)* and bloody diarrhea. This disease is caused by *Turkey Hemorrhagic Enteritis Virus (THEV)* of which avirulent strains (THEV-A) that do not cause HE but retain the immunosuppressive ability have been isolated. The THEV-A Virginia Avirulent Strain (VAS) is still used as a live vaccine despite its immunosuppressive properties. *Our objective is to understand the genetic basis by which VAS induces IS*. The *transcriptome of THEV* was studied to set the stage for further experimentation with specific viral genes that may mediate IS.

Methods: After infecting a turkey B-cell line (MDTC-RP19) with the VAS vaccine strain, samples in triplicates were collected at 4-, 12-, 24-, and 72-hours post-infection. Total RNA was subsequently extracted, and poly-A-tailed mRNA sequencing done. After trimming the raw sequencing reads with the `FastQC`, reads were mapped to the THEV genome using `Hisat2` and transcripts assembled with `StringTie`. An in-house script was used to consolidate transcripts from all time-points, generating the final transcriptome. PCR, gel electrophoresis, and Sanger sequencing were used to validate all identified splice junctions.

INTRODUCTION

Adenoviruses (AdVs) are non-enveloped icosahedral-shaped DNA viruses, causing infection in virtually all vertebrates. Their double-stranded linear DNA genomes range between 26 and 45kb in size, producing a broad repertoire of transcripts via highly complex alternative splicing patterns (1, 2). The AdV genome is one of the most optimally economized; both the forward and reverse DNA strands harbor protein-coding genes, making it highly gene-dense. There are 16 genes termed “genus-common” that are homologous in all AdVs; these are thought to be inherited from a common ancestor. All other genes are termed “genus-specific”. “Genus-specific” genes tend to be located at the termini of the genome while “genus-common” genes are usually central (1). This pattern is observed in *Adenoviridae*, *Poxviridae*, and *Herpesviridae* (1, 3, 4). The family *Adenoviridae* consists of five genera: *Mastadenovirus* (MAdV), *Aviadenovirus*, *Atadenovirus*, *Ichtadenovirus*, and *Siadenovirus* (SiAdV) (5, 6). Currently, there are three recognized members of the genus SiAdV: frog adenovirus 1, raptor adenovirus 1, and turkey adenovirus 3 also called turkey hemorrhagic enteritis virus (THEV) (5, 7–10). Members of SiAdV have the smallest genome size (~26 kb) and gene content (~23 genes) of all known AdVs, and many “genus-specific” putative genes of unknown functions have been annotated (see **Figure 1**)(1, 2, 7).

Virulent THEV strains (THEV-V) and avirulent strains (THEV-A) of THEV are serologically indistinguishable, infecting turkeys, chickens, and pheasants, with the THEV-V causing different clinical diseases in these birds (2, 11). In turkeys, the THEV-V cause hemorrhagic enteritis (HE), a debilitating acute disease affecting predominantly 6-12-week-old turkeys characterized by immunosuppression (IS), weight loss, intestinal lesions leading to bloody diarrhea, splenomegaly, and up to 80% mortality (11–13). HE is the most economically significant disease caused by any strain of THEV (11). While the current vaccine strain (a THEV-A isolated from a pheasant, Virginia Avirulent Strain [VAS]) has proven effective at preventing HE in young turkey poults, it still retains the immunosuppressive ability. Thus, vaccinated birds are rendered more susceptible to opportunistic infections and death than unvaccinated cohorts leading to substantial economic losses (11, 14–16). The induced IS also interferes with vaccination schemes for other infections of turkeys (11, 14). To eliminate this immunossupressive side-effect of the vaccine, a thorough investigation of the culprit viral factors (genes) mediating this phenomenon is essential. However, the transcriptome (splicing and gene expression patterns) of THEV has not been characterized, making the investigation of specific viral genes for possible roles in causing IS impractical. A well-characterized transcriptome of THEV is required to enable experimentation with specific viral genes that may mediate IS.

Myriads of studies have elucidated the AdV transcriptome in fine detail (17, 18). However, a large pre-

ponderance of studies focus on MAdVs — specifically human AdVs. Thus, most of the current knowledge regarding AdV gene expression and replication is based on MAdV studies, which is generalized for all other AdVs (6, 19). MAdV genes are transcribed in a temporal manner; therefore, genes are categorized into five early transcription units (E1A, E1B, E2, E3, and E4), two intermediate (IM) units (pIX and IVa2), and one major late unit (MLTU or major late promoter [MLP] region), which generates five families of late mRNAs (L1-L5) based on the polyadenylation site. An additional gene (UXP or U exon) is located on the reverse strand. The early genes encode non-structural proteins such as enzymes or host cell modulating proteins, primarily involved in DNA replication or providing the necessary intracellular niche for optimal replication while late genes encode structural proteins. The immediate early gene E1A is expressed first, followed by the the delayed early genes, E1B, E2, E3 and E4. Then the intermediate early genes, IVa2 and pIX are expressed followed by the late genes (6, 17, 18). Noteworthily, the MLP shows basal transcriptional activity during early infection (before DNA replication), with a comparable efficiency to other early viral promoters, but reaches its maximal activity during late infection (after DNA replication). However, during early infection the repertoire of late transcripts from the MLP is restricted until late infection (6). MAdV makes an extensive use of alternative RNA splicing to produce a very complex array of mRNAs. All but the pIX mRNA undergo at least one splicing event. The MLTU produces over 20 distinct splice variants all of which contain three non-coding exons at the 5'-end (collectively known as the tripartite leader, TPL) (17, 18). There is also an alternate 5' three non-coding exons present in varying amounts on a subset of MLTU mRNAs (known as the x-, y- and z-leaders). Lastly, there is the i-leader exon, which is infrequently included between the second and third TPL exons, and codes for the i-leader protein (20). Thus, the MLTU produces a complex repertoire of mRNA with diverse 5' untranslated regions (UTRs) spliced onto different 3' coding exons which are grouped into five different 3'-end classes (L1-L5) based on polyadenylation site. Each transcription unit (TU) contains its own promoter driving the expression of all the array of mRNA transcripts produced via alternative splicing in the unit (6, 17, 18). During translation of AdV mRNA, recent studies strongly suggest the potential usage of secondary start codons; adding to what was already a highly complex system for gene expression (17).

High throughput sequencing methods have facilitated the discovery of many novel transcribed regions and splicing isoforms. It is also a very powerful tool to study alternative splicing under different conditions at an unparalleled depth (18, 21). In this paper, a paired-end deep sequencing experiment was performed to characterize for the first time the transcriptome of THEV (VAS vaccine strain) during different phases of the infection, yielding the first THEV splicing map. Our paired-end sequencing allowed for reading **149** bp long high quality (mean Phred Score of 36) sequences from each end of cDNA fragments, which were mapped

to the genome of THEV.

RESULTS

Overview of sequencing data and analysis pipeline outputs

A previous study by Zeinab *et al* showed that almost all THEV transcripts were detectable beginning at 4 hours (22). Therefore, infected MDTC-RP19 cells were harvested at 4-, 12-, 24-, and 72-hours post-infection(h.p.i) to ensure an amply wide time window to sample all transcripts. Our paired-end RNA sequencing (RNA-seq) experiment yielded an average of **107.1** million total reads of **149**bp in length per time-point, which were simultaneously mapped to both the virus (THEV) and host (*M. gallopavo*) genomes using the `Hisat2` (23) alignment program. A total of **18.1** million reads from all time-points mapped to the virus genome; this provided good coverage/depth, leaving no regions unmapped. The mapped reads to the virus genome increased substantially from **432** reads at 4 h.p.i to **16.9** million reads at 72 h.p.i (**Table 1**, **Figure 2a**). From the mapped reads, we identified a total of **2,457** unique THEV splice junctions from all time-points, with splice junctions from the later time-points being supported by significantly more sequence reads than earlier time-points. For example all the **13** unique junctions at 4 h.p.i had less than 10 reads supporting each one, averaging a mere **2.8** reads/junction. Conversely, the **2374** unique junctions at 72 h.p.i averaged **898.4** reads/junction, some junctions having coverage as high as **322,677** reads. The substantial increases in splice junction and mapping reads to the THEV genome over time denotes an active infection, and correlates with our quantitative PCR (qPCR) assay quantifying the total number of viral genome copies over time (**Figure 2b**).

Using `StringTie` (23), an assembler of RNA-seq alignments into potential transcripts, the mapped reads for each time point were assembled into transcripts using the genomic location of the predicted THEV ORFs as a guide. In the consolidated transcriptome, a composite of all unredundant transcripts from all time points, we counted a total of **29** novel transcripts. ~~and using 3' Rapid Amplification of cDNA Ends (3'RACE) and other methods, we further identified #### unique splice variants~~. Although some exons in some transcripts match the predicted ORFs exactly, most of our identified exons are longer, spanning multiple predicted ORFs (**Figure 3**).

We validated the splice junctions in all transcripts by PCR amplification of viral cDNA, cloning, and Sanger sequencing (**Supplementary PCR methods**). The complete list of unique splice junctions mapped to THEV's genome has been submitted to the National Center for Biotechnology Information Gene Expression Omnibus (http://www.ncbi.nlm.nih.gov/geo) under **accession no. XXXXXX**.

Changes in THEV splicing profile over time

AdV gene expression occurs under exquisite temporal control with each promoter typically producing one or

few pre-mRNAs that undergo alternative splicing to yield the manifold repertoire of complex transcripts. To evaluate the activity of each promoter over time, `StringTie` and `Ballgown` (a program for statistical analysis of assembled transcriptomes) (24) were used to estimate and normalize expression levels of all transcripts for each time point in Fragments Per Kilobase of transcript per Million mapped reads (FPKM) units. Very few unique splice junctions, reads, and transcripts were counted at 4 h.p.i; hence, this time point was excluded in this analysis.

Individually, TRXPT_21 (DBP) — from the E2 region — was the most significantly expressed at 12 h.p.i, comprising about **33.58**% of the total transcripts. Transcripts in the E3 and E4 regions also contributed significant proportions, and noticeably, some MLP region transcripts. The later time points were dominated by the MLP region — TRXPT_10 and TRXPT_14 were the most abundantly expressed at 24 and 72 h.p.i, respectively, as expected (**Figure 4a**). When we performed analysis of the FPKM values of transcripts per region we found a similar pattern: the E2 region was the most abundantly expressed at 12 h.p.i, after which the MLP region assumes predominance (**Figure 4b**). Secondly, we estimated relative abundances of all splice junctions at each time point using the raw reads. We counted as significantly expressed only junctions with coverage of at least 1% of the total splice junction reads at the given time point. At 12 h.p.i, **18** junctions meet the 1% threshold, and were comprised of predominantly early region (E1, E2, E3, and E4) junctions, albeit the MLTU was the single most preponderant region overall, constituting **38.8**% of all the junction reads (**Table 2a**). The top most abundant junctions at 12 h.p.i remained the most significantly expressed at 24 h.p.i also. However, here, the MLP-derived junctions were unsurprisingly even more preponderant overall, accounting for **45.7**% of all the junction reads counted (**Table 2b**). At 72 h.p.i, the trend of increased activity of the MLP continued as expected; at this time, the MLP-derived junctions were not only the most abundant overall — accounting for **67.4**% of all junctions reads — but also contained the most significantly expressed individual junctions (**Table 2c**. Also see **Supplementary Tables 1a-c**; **Figure 4c**). When we limited this analysis to only junctions in the final transcriptome, the relative abundances of the junctions for each region over time was generally similar to the pattern seen with all the junctions included (**Figure 4d**).

We also analyzed splice donor and acceptor site nucleotide usage over time to investigate any peculiarities that THEV may show, generally or over the course of the infection. We found that most splice donor-acceptor sequences were unsurprisingly the canonical GU-AG nucleotides.

Early Region 1 (E1) transcripts

This region in MAdVs is the first transcribed after successful entry of the viral DNA into the host cell nucleus, albeit at low levels (18). The host transcription machinery solely mediates the transcription of this region. After their translation, the E1 proteins in concert with a myriad of host transcription factors activate the

other viral promoters (6). Only two ORFs (ORF1 [sialidase] and Hyd) are predicted in this region; however, we discovered **four** novel transcripts in this region, which collectively contain **3** unique splice junctions (**Figure 5**). Most of the encoded proteins of the novel transcripts are distinct from the predicted ORFs, although they all have the potential to encode the predicted Hyd protein as the 3'-most coding sequence (CDS) if secondary start codon usage is considered as reported for other AdVs (17, 18). The 5'-most CDS of TRXPT_1 is multi-exonic, encoding a novel 17.9 kilodalton (kDa), 160 residue [amino acids (aa)] protein. From its 5'-most start codon (SSC), TRXPT_2 encodes the largest protein in this region — a 64.3 kDa, 580 aa protein with the same SSC as TRXPT_1 (position 211bp). This CDS spans almost the entire predicted ORF1 and Hyd, coming short in two regards: it is spliced from 1655 to 1964bp (ORF1's C-terminus, including the stop codon), and it's stop codon (STC; position 2312) is 13 bp short of the Hyd's STC. However, it has an SSC 102 bp upstream and in-frame with ORF1's predicted SSC. Thus, the CDS of TRXPT_2 shares substantial protein sequence similarity with ORF1 but not with Hyd, as the SSC of Hyd is not in-frame. Without its splice site removing the ORF1 STC, TRXPT_2 would encode a longer variant of ORF1, starting from an upstream SSC. TRXPT_3 is almost identical to TRXPT_1, except for the lack of TRXPT_1's second exon. Our RNA-seq data shows that all E1 transcripts share the same transcription termination site (TTS; at position 2325bp); however, TRXPT_3 and TRXPT_4 seem to have transcription start sites (TSS) downstream of the TSS of TRXPT_1 and TRXPT_2 (at position 54bp). Given that studies in MAdVs show that E1 mRNAs share not only a common TTS but also the TSS, and only differ from each other regarding the internal splicing (18), it is likely that TRXPT_3 and TRXPT_4 are incomplete, and their actual TSS just like the TTS are identical for all E1 transcripts. Regardless of the TSS considered for TRXPT_3, the coding potential (CP) remains unaffected. Its 5'-most CDS, beginning at 1965bp and sharing the same STC as TRXPT_1 and TRXPT_2, produces a 13.1 kDa, 115 residue protein (ORF4). ORF4 was predicted in an earlier study (25) but was excluded in later studies (1, 12); however, our data suggests it is a bona fide ORF. Unlike TRXPT_3, the CP of TRXPT_4 is affected by the TSS considered; if we consider its unmodified TSS, then its CP is the same as TRXPT_3 (ORF4 as the first CDS and Hyd as second CDS if the first SSC is skipped). However, if we assume that TRXPT_4 shares the same TSS as TRXPT_1, then the 5'-most CDS is a distinct, novel, multi-exonic 15.9 kDa, 143 aa protein with the same SSC as TRXPT_1 and TRXPT_2 but with a unique STC. The splice junctions of the transcripts in this region (except the junction for TRXPT_4) were validated by cloning of viral cDNA and Sanger sequencing (**Figure 5**; **Supplementary PCR methods**). During the validation of TRXPT_2, ORF1 was present on the agarose gel (an unspliced band size) and Sanger sequencing results as a bona fide transcript (**Supplementary PCR methods**). This was corroborated by our 3'RACE experiment, which showed a transcript (TRXPT_2B) spanning the entire ORF1 and Hyd ORFs without any splicing, with a poly-A tail immediately after the TTS of transcripts in this

region. The 5'-most CDS of this transcript (TRXPT_2B) would encode ORF1. However, TRXPT_2B has an upstream and in-frame SSC to the predicted SSC of ORF1, suggesting that the predicted ORF1 CDS is truncated; it shares the same TSS, SSC, and TTS as TRXPT_2, but has a unique STC.

Early Region 2 (E2) and Intermediate Region (IM) transcripts

The E2 TU expressed on the anti-sense strand, is subdivided into E2A and E2B and encodes three classical AdV proteins essential for genome replication: pTP and Ad-pol (E2B proteins), and DBP (E2A protein) (17, 18). Unlike MAdV where two promoters (E2-early and E2-late) are known (17), we discovered only a single TSS (E2 TSS; 18,751bp) from which both E2A and E2B transcription is initiated. However, similar to MAdVs, E2A and E2B transcripts have distinct TTSs, and the E2B transcripts share the TTS of the IVa2 transcript of the IM region (17, 18) (**Figure 6**).

The E2A ORF, DBP is one of three THEV ORFs predicted to be spliced from two exons. The corresponding transcript (TRXPT_21) found in our data matches this predicted splicing pattern precisely but with a non-coding additional exon at the 5'-end (E2-5'UTR) at position 18,684-18,751 bp. Thus, TRXPT_21 is a three-exon transcript encoding DBP (380 residues, 43.3 kDa) precisely as predicted. This transcript (TRXPT_21) was also corroborated in a 3'-RACE experiment. Additionally, from the 3'-RACE, a splice variant of TRXPT_21 which retains the second intron leading to a 2-exon transcript was found. This transcript (TRXPT_21B), albeit longer due to retaining the second intron and possessing a short 3' UTR, encodes a truncated isoform of DBP because the first SSC utilized by TRXPT_21, is followed shortly by STCs in the retained intron, and does not yield any viable product. Utilizing the SSC 173 bp downstream of TRXPT_21's SSC yields a 346 residue, 39.3 kDa product, which is in-frame of DBP but entirely contained in the second exon. TRXPT_21 and TRXPT_21B share a common TTS but TRXPT_21B as seen in our 3'-RACE data, extends 39 bp into an adenine-thymine (A-T) rich sequence before the poly-A tail sequence occur, suggesting this position (16,934bp) as the bona fide E2A TTS (**Figure 6**).

The E2B region transcripts also start with the E2-5'UTR but extend thousands of base pairs downstream to reach the TTS at 2334bp in the IM region, which is immediately followed by an A-T rich sequence (position 2323-2339bp) where polyadenylation probably occurs. Interestingly, the TTS of the E1 region (position 2,325bp) on the sense strand is also in the immediate vicinity of this A-T rich sequence, which is almost palindromic; hence it likely serves as the polyadenylation signal for both E1 and E2B/IM transcripts. The E2B transcripts, TRXPT_6 and TRXPT_7 are almost identical except for an extra splice junction at the 3'-end of TRXPT_6, making TRXPT_6 a five-exon transcript and TRXPT_7, four exons (**Figure 6**). TRXPT_7 has the CP for IVa2 and both classical proteins (pTP and Ad-pol) encoded in this region, of which the pTP ORF is predicted to be spliced from two exons just like in all other AdVs. The predicted splice junction of

pTP is corroborated by our data; however, the full transcript is markedly longer than the predicted ORF: there are two novel non-coding 5' exons, the third exon (containing the SSC of pTP) is significantly longer than predicted, and the last exon containing the bulk of the CDS is more than triple the predicted size of pTP. The first two exons are 5'-UTRs because the SSC here is immediately followed by STCs; hence, the 5'-most SSC (position 10,995bp) of the third exon which matches the predicted SSC of pTP is utilized. The encoded product is identical to the predicted pTP ORF (597 residues; 70.5 kDa). If secondary SSC (secSSC) usage is considered, with SSC at 6768bp and STC at 3430bp, the encoded product is identical to the predicted Ad-pol (polymerase) ORF (1112 residues; 129.2 kDa). TRXPT_6 differs from TRXPT_7 by containing an extra splice site at 3447-3515bp. However, the CP remains similar to that of TRXPT_7 except the Ad-pol encoded from the secSSC is a truncated isoform with a new STC resulting from the splice site. We also found a novel short transcript (TRXPT_15) entirely nested within the terminal exon of TRXPT_7 but with a unique splice site. This transcript is an incomplete construction from the mapped reads as it contains an incomplete CDS. However, we validated the this splice junction to be genuine (**Supplementary PCR methods**).

The IM region is a single-transcript TU, encoding a single classical protein, IVa2. The promoter expressing this single transcript (TRXPT_5) is embedded in E2B region and shares a TTS with E2B transcripts (17, 18). TRXPT_5 is a two-exon transcript spliced at 3447-3615bp exactly as the last intron of TRXPT_6. The first exon is an UTR, except the last 2 nucleotides, which connect with the first nucleotide of second exon to form the 5'-most SSC. This first SSC is 4 codons upstream and in-frame of the predicted IVa2 SSC. Regardless of the SSC considered, the encoded protein (IVa2) is largely unaffected. Except for the four extra residues at the N-terminus (considering the 5'-most SSC), the entire protein sequence is identical to IVa2.

Early Region 3 (E3) transcripts.

The E3 region is wholly contained in the MLTU and encodes proteins involved in modulating and evading the host immune defenses. In MAdVs, this region contains seven ORFs expressed from several transcripts which share the same TSS (from the E3 promoter) but have different TTSs (6, 17, 18). However, some E3 transcripts use the TSS of the MLP. Due to sharing the same TSS, in MAdVs, secSSC usage is heavily relied on for gene expression in this region except for 12.5K and transcripts using the MLP's TSS, as utilizing only the first SSC cannot produce all the other transcripts in this TU (17).

In THEV, only one ORF (E3) was predicted in this region. However, we identified six novel transcripts here (**TRXPT_22, TRXPT_23, TRXPT_24, TRXPT_25, TRXPT_26, TRXPT_27**) (**Figure 7**). We identified two distinct TSSs — one similar to the classic MAdV E3 TSS (position 18,230bp) and the other about

500 bp downstream at 18,727bp. The E3 transcripts collectively have the CP for several predicted THEV ORFs: 100K, 22K, 33K, pVIII, E3, Fiber (IV), and ORF7 belonging to the MLTU; however, some CDSs are nonidentical due to unpredicted splicing or the use of an upstream, in-frame SSC. For instance, 33K is one of the few THEV ORFs predicted to be spliced from two exons; however, we discovered it to be a significantly longer four-exon ORF expressed from TRXPT_24. The first two exons of L33K were not predicted but the last two match the predicted exons and the CDS is in-frame. However, the first 20bp of the predicted 33K (including the SSC at 20,142bp) is spliced out as as part of the second intron of TRXPT_24. Thus, the bona fide 33K is a 19.8 kDa, 171 residue protein (L33K) spanning four exons instead of the predicted 120 aa protein. TRXPT_24 also has the CP for the ORFs, pVIII and E3 (a longer variant starting from and upstream, in-frame SSC) if we consider downstream SSC usage. Also, 22K (89 residues) is a single-exon ORF predicted to use the same SSC as 33K (20,142bp). However, just like 33K, all the transcripts in this region exclude the predicted SSC as part of their introns; hence 22K as predicted is not identical to any expressed ORF. TRXPT_29 has its SSC upstream of 22K's predicted SSC but is spliced to overlap a portion of 22K's CDS. However, the overlapping sequence is short and not in-frame of 22K. The 5'-most product of TRXPT_29 is a novel 73 residue protein (8.3aK) entirely different from 22K. TRXPT_23 being spliced identically as TRXPT_29 also encodes this novel 73 aa protein (8.3aK) from its first SSC. Similarly, TRXPT_22 also encodes a 73 aa novel protein (8.3bK) from its first SSC that shares over 80% similarity with 8.3aK, but it differs from 8.3aK at the C-terminus. Considering downstream SSC usage, both TRXPT_22 and TRXPT_23 can encode pVIII and E3 in that order, but TRXPT_23 being longer, has the CP for the Fiber ORF also. As the splice junctions of TRXPT_22, TRXPT_23, TRXPT_24, and TRXPT_29 essentially share the same genomic space, their validation was done with a single primer pair and they were differentiated from each other by cloning and Sanger sequencing.

In addition to corroborating the splice junctions for the aforementioned transcripts, the Sanger sequencing results also showed another splice variant undetected in our RNA-seq transcriptome. This was a three-exon transcript (TRXPT_30) with its first and last exons spliced identically as TRXPT_23, but which also has the second exon of TRXPT_24 (**Figure 7**). The first CDS on TRXPT_30 spans all three exons, with the STC in the terminal (third) exon, producing a novel 140 residue, 15.7kDa protein (L22K). Interestingly, the last 81 C-terminus residues are identical to 22K (89 residues); only the first 7 residues are lacking due to splicing. Hence, we may consider L22K as a long variant of the predicted 22K ORF. Albeit the TSS and TTS of TRXPT_30 was not seen, we presume that they are similar to TRXPT_23, in which case it would also have the downstream CP of TRXPT_23. TRXPT_25 is the largest transcript in the TU. It also utilizes the classic E3 TSS but has distinct TTS. It is a two exon transcript, encoding a novel protein (t100K; 543 residues),

which is a shorter isoform of the predicted 100K ORF. Considering secSSC usage on this transcript yields the predicted ORF, 22K. It also has the CP for pVIII and E3 in that order. Furthermore, during the validation of TRXPT_25's splice junction using primers that span its junction (18350-18717bp), we noticed a DNA band that corresponds to the full unspliced sequence (**Supplementary PCR methods**). As TRXPT_25 only falls short of encoding the complete predicted 100K protein due to its splice junction, this band (which we cloned and validated by Sanger sequencing) suggests that the predicted 100K is indeed expressed. This transcript (TRXPT_25B) although not seen in our RNA-seq data, likely shares the same TSS and TTS as TRXPT_25. Lastly, TRXPT_26 and TRXPT_27 share the same TSS, unique from the other transcripts in this region but with distinct TTSs. TRXPT_26 is a three-exon transcript but the first two are UTRs. It encodes pVIII as the 5'-most ORF and has the CP for E3 and Fiber in that order. TRXPT_27 on the other hand, is only a two-exon transcript but similar to TRXPT_26, only the terminal exon contains the CDSs. It encodes Fiber as the 5'-most ORF, and ORF7 downstream with secSSC usage. TRXPT_13, which seems to be an E3 transcript that uses the MLP TSS is discussed under the MLTU transcripts.

Early Region 4 (E4) transcripts. This transcription unit (TU) is the found at the tail-end (3'-end) of the genome on the anti-sense strand. Based on nucleotide position, ORF7 and ORF8 were predicted in this region (1); however, as ORF7 is neither on the same strand as ORF8 nor transcribed from a promoter in the E4 region, only ORF8 can legitimately be classified as a transcript in this TU. This is corroborated by our RNA-seq data, as only one transcript was identified in this region on the anti-sense strand (**Figure 8**). The transcript (TRXPT_28) spans 25192-26247 and is spliced at 25701-26055; hence, a two-exon transcript. The second exon fully matches the predicted ORF8 with 12 extra base pairs at the 3'-end; however, the encoded protein is an exact match. There is a SSC in the first exon at position 26246 (second nucleotide of the transcript). The encoded protein from this SSC is in-frame with the predicted SSC of ORF8 in the second exon; hence, the bulk of this longer protein (26.4 kDa, 229 aa) is identical to the predicted ORF8 protein.

Major Late Transcription Unit (MLTU) or MLP Region transcripts

The MLTU transcripts dominate the late phase (i.e, after DNA replication) of the AdV infectious cycle. The MLP produces all late mRNAs by alternative splicing and alternative polyadenylation of a primary transcript, which are grouped into five transcript classes (L1-L5). These late proteins primarily act as capsid proteins, promote virion assembly, and direct genome packaging (6, 17, 18). Similar to other AdVs, most of THEV's coding capacity falls within this TU. Specifically, about 13 out of the 23 predicted ORFs were assigned to this TU, some of which we have found to belong to the E3 TU instead. Our RNA-seq data revealed 12 transcripts (**TRXPT_8, TRXPT_9, TRXPT_10, TRXPT_11, TRXPT_12, TRXPT_13, TRXPT_14, TRXPT_16,**

TRXPT_17, TRXPT_18, TRXPT_19, TRXPT_20) in this TU. We identified the untranslated TPL at the 5' end of most transcripts in this region as expected. However, for three transcripts (**TRXPT_16, TRXPT_17, TRXPT_18**), a different leader sequence (sTPL) is used: the first TPL exon is substituted for a unique first exon, found between the first and second TPL exons. Also, TRXPT_20 seems to include only the third TPL exon (**Figure 9**).

We identified five TTSs (10,549bp, 12,709bp, 16,870bp, 17,891bp, 20,865bp) in this TU, corresponding to the five late mRNA classes (L1-L5), respectively, as found in all AdVs. L1 mRNAs include TRXPT_8, which comprises the TPL (non-coding) and the CDS-containing terminal exon. This transcript encodes the 52K ORF exactly as predicted with the SSC beginning from the first nucleotide of the terminal exon. L2 mRNAs include TRXPT_16, TRXPT_17, and TRXPT_18, all of which consist of the sTPL (also non-coding) followed by their respective terminal exons. TRXPT_16 encodes pIIIa exactly as predicted as the 5'-most ORF, and also has the CP for the ORFs, III and pVII in that order. TRXPT_17 encodes the ORF, III (penton), and TRXPT_18 encodes the ORF pVII exactly as predicted. The L3 mRNAs include TRXPT_14 and TRXPT_20, of which TRXPT_14 utilizes the full TPL whereas TRXPT_20 uses only the third TPL exon (ex3TPL). Both transcripts have the CP for the ORF, hexon (II) but hexon is the only ORF encoded on TRXPT_14, whereas the 5'-most ORF on TRXPT_20 is pX (pre-Mu) followed by pVI and hexon in that order. L4 mRNAs include TRXPT_9, TRXPT_10, TRXPT_11, and TRXPT_13 all of which begin with the TPL followed by three (TRXPT_9, TRXPT_10, and TRXPT_13) or four (TRXPT_11) coding exons. These are the largest transcripts found in the transcriptome, each one possessing the CP for several similar late proteins. Normally, MLTU transcripts encoding particular ORFs splice the TPL onto a splice site just upstream of the ORF to be expressed (17). While this holds true for most MLTU ORFs, several late ORFs (pVI, protease, and ORF7) do not have such close proximity splicing but are contained in larger transcripts such as the L4 mRNAs, strongly suggesting the use of non-standard ribosomal initiation mechanisms such as secSSC utility and ribosome shunting found in other AdVs for their translation (17, 26). TRXPT_9 and TRXPT_10 are very similar but not identical. The last exon of TRXPT_9 seems to be truncated and probably shares the same TTS as the other L4 mRNAs. They are both 6-exon transcripts encoding pVII as the 5'-most ORF (fourth exon) and also have the CP for pX, pVI, hexon, a longer variant of protease (Lprot) — uses an in-frame, upstream SSC than predicted, and 14K (a novel unpredicted 120 aa protein). TRXTP_10 (and TRXPT_9 with the L4 TTS) also has the CP for pVIII and E3. TRXPT_11 is a seven-exon mRNA with hexon as it's 5'-most ORF but it also has the CP for Lprot, 14K, L33K, and also pVIII and E3 in that order. TRXPT_13 seems to be an E3 ORF utilizing the MLP TSS. It encodes pVIII and E3 in that order similar to TRXPT_22 but lacks TRXPT_22's novel first ORF.

Lastly, the L5 class includes only TRXPT_12 which contains the TPL and a coding terminal exon. Its 5'-most ORF is fiber (IV) but it also has the CP for the THEV specific gene, ORF7. TRXPT_12's CP is identical TRXPT_27 of the the E3 TU albeit they differ in their 5'-UTRs.

DISCUSSION/CONCLUSIONS

For fig2a: There is a dramatic increase of mean coverage/depth from **2.42** at 4 h.p.i to **95,042** at 72 h.p.i, strongly demonstrating an active infection. Unexpectedly, the pileup of reads seems consistently skewed over similar regions of the genome. We could speculate that the temporal gene expression regulation of THEV is different from MAdVs or this could simply mean that the infection was not well synchronized. However, the relative proportions over these similar regions shows some variation over time. For fig2b: titer reaching a plateau at 120 h.p.i, probably due to high cell death TRXPT_2 and ORF1 are isoforms Presumably, if the junction reads were normalized, MLTU would not be predominant at 12hpi. The TTSs were all in the context of A-T rich sequences; which presumably serve as polyA signals. All splice junctions were confirmed by cloning and Sanger sequencing of cDNA (**Supplementary PCR methods**). We did not find the x,y,z or i-leaders for MLP transcripts probably because THEV doesn't use it due to its smaller size The E3 ORF has an upstream, in-frame SSC.

MATERIALS AND METHODS

Cell culture and THEV Infection

The Turkey B-cell line (MDTC-RP19, ATCC CRL-8135) was grown as suspension cultures in 1:1 complete Leibovitz's L-15/McCoy's 5A medium with 10% fetal bovine serum (FBS), 20% chicken serum (ChS), 5% tryptose phosphate broth (TPB), and 1% antibiotics solution (100 U/mL Penicillin and 100ug/mL Streptomycin), at 41°C in a humidified atmosphere with 5% CO_2. Infected cells were maintained in 1:1 serum-reduced Leibovitz's L15/McCoy's 5A media (SRLM) with 2.5% FBS, 5% ChS, 1.2% TPB, and 1% antibiotics solution (100 U/mL Penicillin and 100ug/mL Streptomycin). A commercially available HE vaccine was purchased from Hygieia Biological Labs as a source of THEV-A (VAS strain). The stock virus was titrated using an in-house qPCR assay with titer expressed as genome copy number(GCN)/mL, similar to Mahshoub *et al* (27) with modifications. Cells were infected at a multiplicity of infection (MOI) of 100 GCN/cell and samples in triplicates were harvested at 4-, 12-, 24-, and 72-h.p.i for RNA-seq. The infection was repeated but samples in triplicates were harvested at 12-, 24-, 36-, 48-, and 72-h.p.i for PCR validation of novel splice sites. Still one more independent infection was done at time points ranging from 12 to 168-h.p.i for qPCR quantification of virus titers.

RNA extraction and Sequencing

Total RNA was extracted from infected cells using Thermofishers' RNAqueous™-4PCR Total RNA Isolation Kit `(#AM1914)` per manufacturer's instructions. An agarose gel electrophoresis was performed to check RNA integrity. The RNA quantity and purity was initially assessed using `nanodrop`, and RNA was used only if the A260/A280 ratio was 2.0 ± 0.05 and the A260/A230 ratio was >2 and <2.2. Extracted total RNA samples were sent to `LC Sciences, Houston TX` for poly-A-tailed mRNA sequencing where RNA integrity was checked with `Agilent Technologies 2100 Bioanalyzer High Sensitivity DNA Chip` and poly(A) RNA-seq library was prepared following `Illumina's TruSeq-stranded-mRNA sample preparation protocol`. Paired-end sequencing was performed on `Illumina's NovaSeq 6000 sequencing system`.

Validation of Novel Splice Junctions

All splice junctions identified in this work are novel except one predicted splice site each for pTP and DBP, which were corroborated in our work. However, these predicted splice junctions had not been experimentally validated hitherto, and we identified additional novel exons, giving the complete picture of these tran-

scripts. The novel splice junctions in this work discovered in the assembled transcripts using the StringTie transcript assembler which we validated by PCR and Sanger Sequencing are shown in **Supplementary PCR methods**. Briefly, we designed primers that crossed a range of novel exon-exon boundaries for each specific transcript in a transcription unit (TU) paired with their respective universal primers for the TU. Each forward primer contained a KpnI restriction site and reverse primers, an XbaI site. After first-strand cDNA synthesis with SuperScript™ III First-Strand Synthesis System, these primers were used in a targeted PCR amplification, the products analyzed with agarose gel electrophoresis to confirm expected band sizes, cloned by traditional restriction enzyme method, and Sanger sequenced to validate these splice junctions at the sequence level.

3' Rapid Amplification of cDNA Ends (3'-RACE)

We performed a rapid amplification of sequences from the 3' ends of mRNAs (3'-RACE) experiment using a portion of the extracted total RNA of infected MDTC-RP19 cells used for the RNA-seq experiment as explained above. We followed the protocol described by Green *et al* (28) with modifications. Briefly, 1ug of total RNA was reverse transcribed to cDNA using SuperScript™ IV First-Strand Synthesis System following the manufacturing instructions using an adapter-primer with a 3'-end poly(T) and a 5'-end BamHI restriction site. A gene-specific sense primer with a 5'-end KpnI restriction site paired with an anti-sense adapter-primer with a 5'-end BamHI site were used to amplify target sections of the cDNA using Invitrogen's Platinum™ Taq DNA polymerase High Fidelity, following manufacturer's instructions. The PCR amplicons were restriction digested, cloned, and Sanger sequenced.

Computational Analysis of RNA Sequencing Data: Mapping and Transcript characterization

Our sequence reads were analyzed following a well established protocol described by Pertea *et al* (23), using `Snakemake - version 7.24.0` (29), a popular workflow management system to drive the pipeline. Briefly, sequencing reads were trimmed with the `FastQC - version 0.11.9` (30) program to achieve an overall `Mean Sequence Quality (Phred Score)` of 36. Trimmed reads were mapped simultaneously to the complete genomic sequence of avirulent turkey hemorrhagic enteritis virus strain Virginia (https://www.ncbi.nlm.nih.gov/nuccore/AY849321.1/) and *Meleagris gallopavo* (https://www.ncbi.nlm.nih.gov/genome/?term=Meleagris+gallopavo) using `Hisat2 - version 2.2.1` (23) with default settings. The generated alignment (`BAM`) files from each infection time point were filtered for reads mapping to the THEV genome and fed into `StringTie - version 2.2.1` (23) using a `GTF` file derived from a `gff3` file obtained from NCBI, which con-

tains the predicted ORFs of THEV as a guide. A custom script was used to consolidate all transcripts from all time-points without redundancy, generating the transcriptome of THEV. See **Supplementary Computational Analysis** for the details of transcript expression level estimations and splice junction read counts.

SCRIPTS AND SUPPLEMENTARY MATERIALS

DATA AVAILABILITY

CODE AVAILABILITY

All the code/scripts written for analysis of the data are available on github (https://github.com/Abraham-Quaye/thev_transcriptome)

ACKNOWLEDGMENTS

LC Sciences - RNA sequencing was done here

Eton Bioscience, Inc, San Diego, CA - All Sanger sequencing validations was done here

REFERENCES

1. Davison A, Benko M, Harrach B. 2003. Genetic content and evolution of adenoviruses. The Journal of general virology 84:2895–908.

2. Harrach B. 2008. Adenoviruses: General features, p. 1–9. *In* Mahy, BWJ, Van Regenmortel, MHV (eds.), Encyclopedia of virology (third edition). Book Section. Academic Press, Oxford.

3. Upton C, Slack S, Hunter AL, Ehlers A, Roper RL. 2003. Poxvirus orthologous clusters: Toward defining the minimum essential poxvirus genome. Journal of virology 77:7590–7600.

4. McGeoch D, Davison AJ. 1999. Chapter 17 - the molecular evolutionary history of the herpesviruses, p. 441–465. *In* Domingo, E, Webster, R, Holland, J (eds.), Origin and evolution of viruses. Book Section. Academic Press, London.

5. Harrach B, Benko M, Both GW, Brown M, Davison AJ, Echavarría M, Hess M, Jones M, Kajon A, Lehmkuhl HD, Mautner V, Mittal S, Wadell G. 2011. Family adenoviridae. Virus Taxonomy: 9th Report of the International Committee on Taxonomy of Viruses 125–141.

6. Guimet D, Hearing P. 2016. 3 - adenovirus replication, p. 59–84. *In* Curiel, DT (ed.), Adenoviral vectors for gene therapy (second edition). Book Section. Academic Press, San Diego.

7. Kovács ER, Benkő M. 2011. Complete sequence of raptor adenovirus 1 confirms the characteristic genome organization of siadenoviruses. Infection, Genetics and Evolution 11:1058–1065.

8. Davison AJ, Wright KM, Harrach B. 2000. DNA sequence of frog adenovirus. J Gen Virol 81:2431–2439.

9. Kovács ER, Jánoska M, Dán Á, Harrach B, Benkő M. 2010. Recognition and partial genome characterization by non-specific DNA amplification and PCR of a new siadenovirus species in a sample originating from parus major, a great tit. Journal of Virological Methods 163:262–268.

10. Katoh H, Ohya K, Kubo M, Murata K, Yanai T, Fukushi H. 2009. A novel budgerigar-adenovirus belonging to group II avian adenovirus of siadenovirus. Virus Research 144:294–297.

11. Beach NM. 2006. Characterization of avirulent turkey hemorrhagic enteritis virus: A study of the molecular basis for variation in virulence and the occurrence of persistent infection. Thesis.

12. Beach NM, Duncan RB, Larsen CT, Meng XJ, Sriranganathan N, Pierson FW. 2009. Comparison of 12 turkey hemorrhagic enteritis virus isolates allows prediction of genetic factors affecting virulence. J Gen Virol 90:1978–85.

13. Gross WB, Moore WE. 1967. Hemorrhagic enteritis of turkeys. Avian Dis 11:296–307.

14. Rautenschlein S, Sharma JM. 2000. Immunopathogenesis of haemorrhagic enteritis virus (HEV) in turkeys. Dev Comp Immunol 24:237–46.

15. Larsen CT, Domermuth CH, Sponenberg DP, Gross WB. 1985. Colibacillosis of turkeys exacerbated by hemorrhagic enteritis virus. Laboratory studies. Avian Dis 29:729–32.

16. Dhama K, Gowthaman V, Karthik K, Tiwari R, Sachan S, Kumar MA, Palanivelu M, Malik YS, Singh RK, Munir M. 2017. Haemorrhagic enteritis of turkeys – current knowledge. Veterinary Quarterly 37:31–42.

17. Donovan-Banfield I, Turnell AS, Hiscox JA, Leppard KN, Matthews DA. 2020. Deep splicing plasticity of the human adenovirus type 5 transcriptome drives virus evolution. Communications Biology 3:124.

18. Zhao H, Chen M, Pettersson U. 2014. A new look at adenovirus splicing. Virology 456-457:329–341.

19. Wolfrum N, Greber UF. 2013. Adenovirus signalling in entry. Cell Microbiol 15:53–62.

20. Falvey E, Ziff E. 1983. Sequence arrangement and protein coding capacity of the adenovirus type 2 "i" leader. Journal of Virology 45:185–191.

21. Djebali S, Davis CA, Merkel A, Dobin A, Lassmann T, Mortazavi A, Tanzer A, Lagarde J, Lin W, Schlesinger F, Xue C, Marinov GK, Khatun J, Williams BA, Zaleski C, Rozowsky J, Röder M, Kokocinski F, Abdelhamid RF, Alioto T, Antoshechkin I, Baer MT, Bar NS, Batut P, Bell K, Bell I, Chakrabortty S, Chen X, Chrast J, Curado J, Derrien T, Drenkow J, Dumais E, Dumais J, Duttagupta R, Falconnet E, Fastuca M, Fejes-Toth K, Ferreira P, Foissac S, Fullwood MJ, Gao H, Gonzalez D, Gordon A, Gunawardena H, Howald C, Jha S, Johnson R, Kapranov P, King B, Kingswood C, Luo OJ, Park E, Persaud K, Preall JB, Ribeca P, Risk B, Robyr D, Sammeth M, Schaffer L, See L-H, Shahab A, Skancke J, Suzuki AM, Takahashi H, Tilgner H, Trout D, Walters N, Wang H, Wrobel J, Yu Y, Ruan X, Hayashizaki Y, Harrow J, Gerstein M, Hubbard T, Reymond A, Antonarakis SE, Hannon G, Giddings MC, Ruan Y, Wold B, Carninci P, Guigó R, Gingeras TR. 2012. Landscape of transcription in human cells. Nature 489:101–108.

22. Aboezz Z, Mahsoub H, El-Bagoury G, Pierson F. 2019. In vitro growth kinetics and gene expression analysis of the turkey adenovirus 3, a siadenovirus. Virus Research 263:47–54.

23. Pertea M, Kim D, Pertea GM, Leek JT, Salzberg SL. 2016. Transcript-level expression analysis of RNA-seq experiments with HISAT, StringTie and ballgown. Nature Protocols 11:1650–1667.

24. Jack Fu [Aut], Alyssa C. Frazee [Aut, Cre], LeonardoCollado-Torres [Aut], Andrew E. Jaffe [Aut], Jeffrey T. Leek[Aut, Ths]. 2017. Ballgown. Bioconductor.

25. Pitcovski J, Mualem M, Rei-Koren Z, Krispel S, Shmueli E, Peretz Y, Gutter B, Gallili GE, Michael A, Goldberg D. 1998. The complete DNA sequence and genome organization of the avian adenovirus, hemorrhagic enteritis virus. Virology 249:307–315.

26. Yueh A, Schneider RJ. 1996. Selective translation initiation by ribosome jumping in adenovirus-infected and heat-shocked cells. Genes & Development 10:1557–1567.

27. Mahsoub HM, Evans NP, Beach NM, Yuan L, Zimmerman K, Pierson FW. 2017. Real-time PCR-based infectivity assay for the titration of turkey hemorrhagic enteritis virus, an adenovirus, in live vaccines. Journal of Virological Methods 239:42–49.

28. Green MR, Sambrook J. 2019. Rapid amplification of sequences from the 3' ends of mRNAs: 3'-RACE. Cold Spring Harbor Protocols 2019:pdb.prot095216.

490 29. Mölder F, Jablonski KP, Letcher B, Hall MB, Tomkins-Tinch CH, Sochat V, Forster J, Lee S, Twardziok SO, Kanitz A, Wilm A, Holtgrewe M, Rahmann S, Nahnsen S, Köster J. 2021. Sustainable data
491 analysis with snakemake. F1000Research 10:33.

492 30. 2015. FastQC.

493

TABLES AND FIGURES

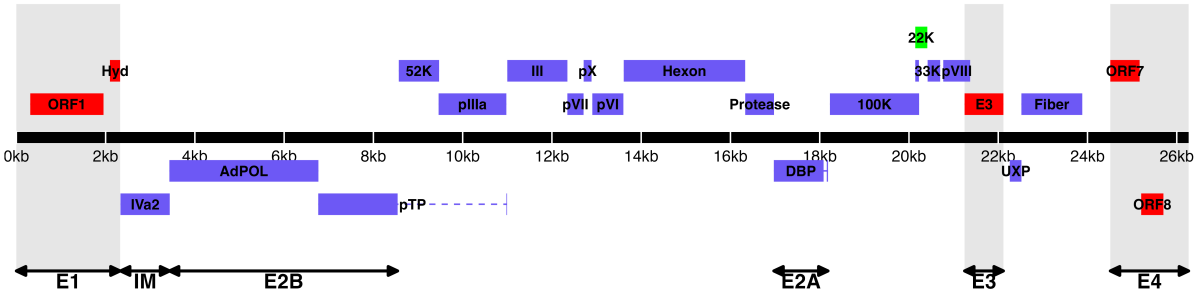

Figure 1. ***Genomic map of THEV avirulent strain annotated ORFs***. The central horizontal line represents the double-stranded DNA marked at 5kb intervals as white line breaks. Blocks represent viral genes. Blocks above the DNA line are transcribed rightward, those below are transcribed leftward. pTP, DBP and 33K predicted to be spliced are shown as having tails. Shaded regions indicate regions containing "genus-specific" genes (colored red). Genes colored in blue are "genus-common". Gene colored in light green is conserved in all but Atadenoviruses. The UXP (light blue) is an incomplete gene present in almost all AdVs. Regions comprising the different transcription units are labelled at the bottom (E1, E2A, E2B, E3, E4, and IM); the unlabeled regions comprise the MLTU.

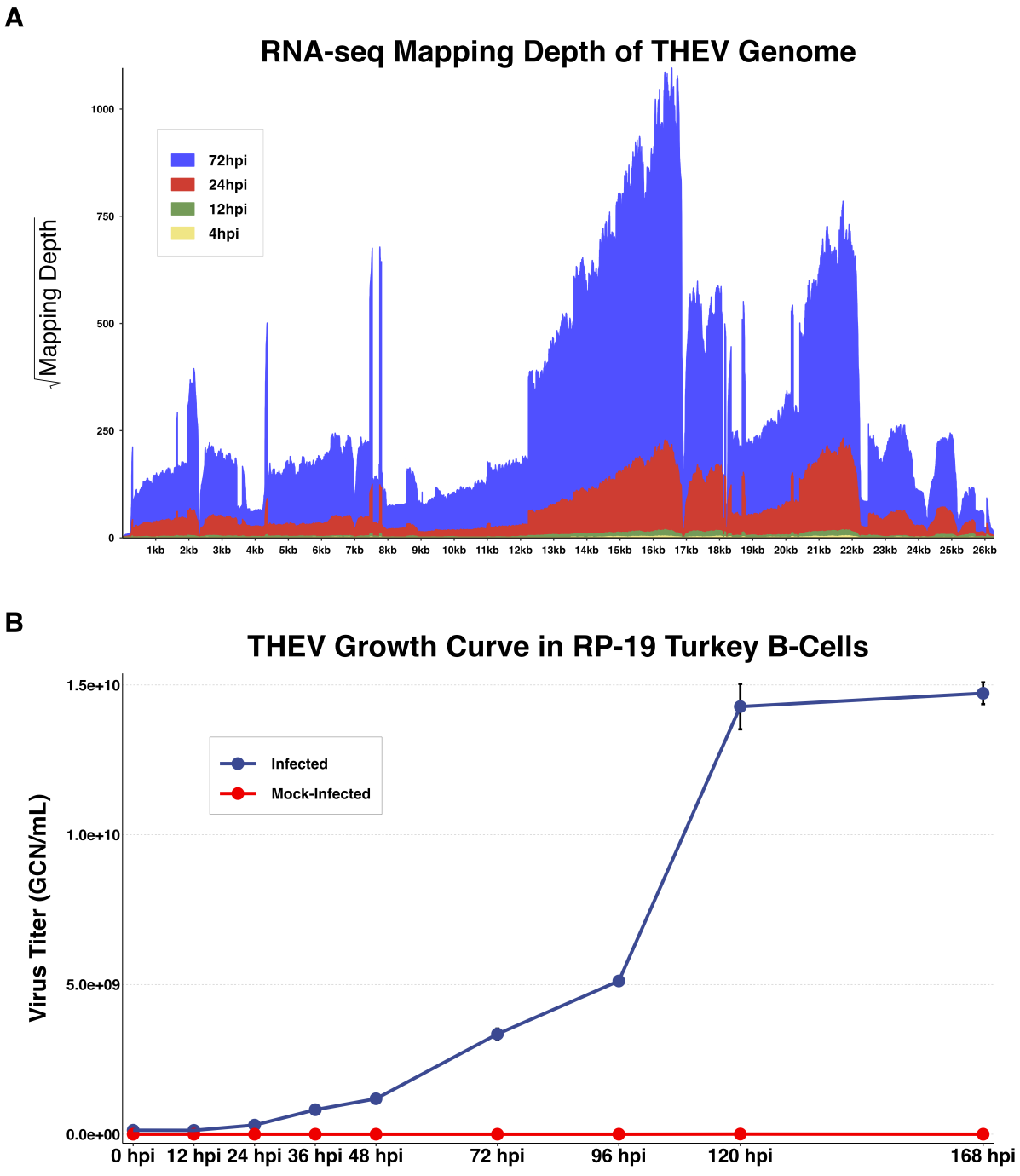

Figure 2: Increasing levels of THEV over time. a) ***Per base coverage of sequence reads mapping to THEV genome by time point***. The pileup of mRNA reads mapping to THEV genome at the base-pair level for each indicated time point. **b)** ***Growth curve of THEV (VAS vaccine strain) in MDTC-RP19 cell line***. Virus titers were a quantified with a qPCR assay. There is no discernible increase in virus titer up 12 h.p.i, after which a steady increase in virus titer is measured. The virus titer expands exponentially beginning

from 48 h.p.i, increasing by orders of magnitude before reaching a plateau at 120 h.p.i. GCN: genome copy number.

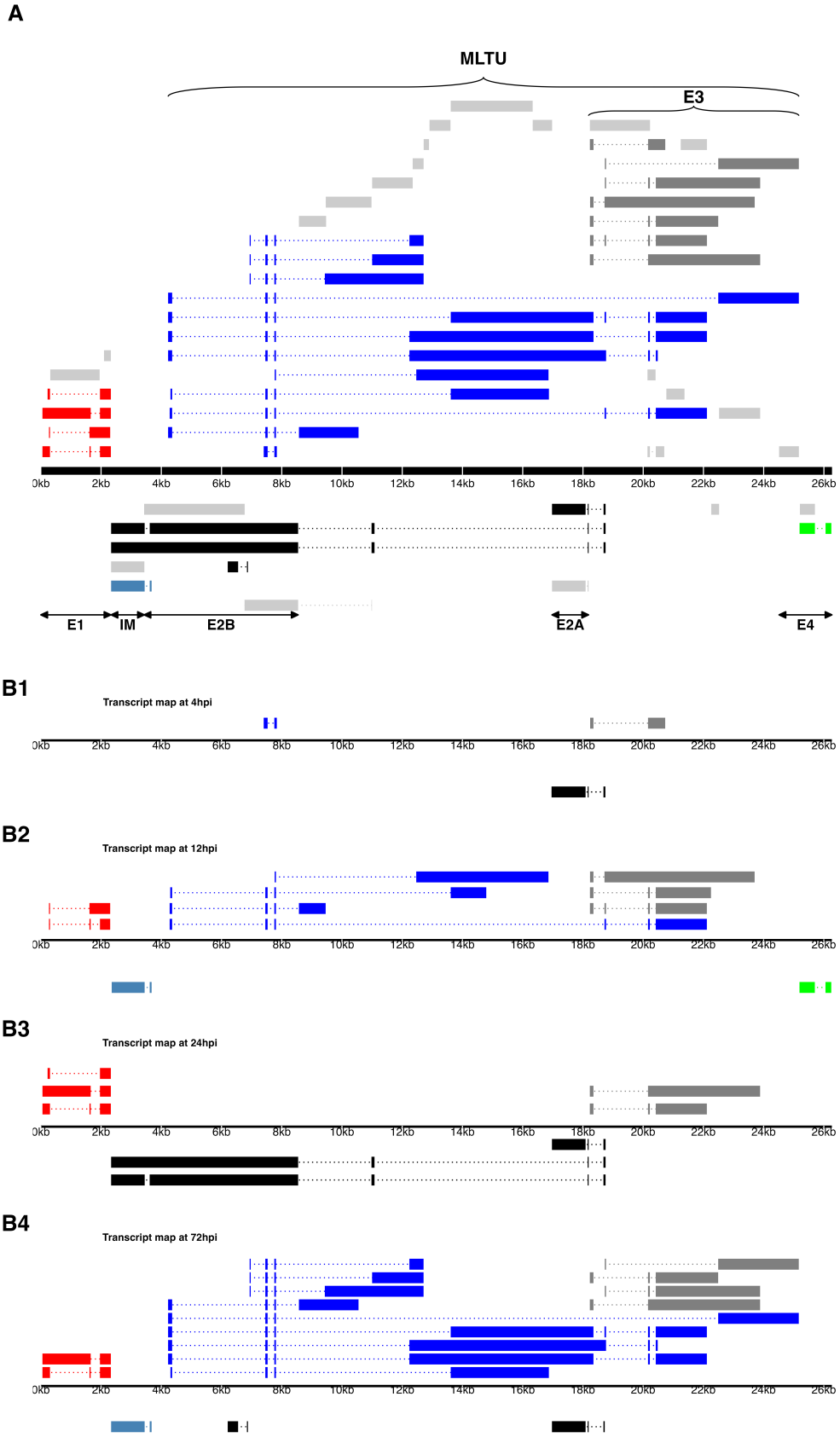

512

Figure 3. a)

Transcriptome of THEV from RNA-seq. THEV transcripts assembled from all time points by `StringTie` are unified forming this final transcriptome (splicing map). Transcripts belonging to the same transcription unit (TU) are located in close proximity on the genome and are color coded and labeled in this figure as such. The organization of TUs in the THEV genome is unsurprisingly similar to MAdVs; however, the MAdV genome shows significantly more transcripts. The TUs are color coded: E1 transcripts - red, E2 - black, E3 - dark grey, E4 - green, MLTU - blue. Predicted ORFs are also indicated here, colored light grey. **b) THEV transcripts identified at given time points**. Transcripts are color coded as explained in **a**.

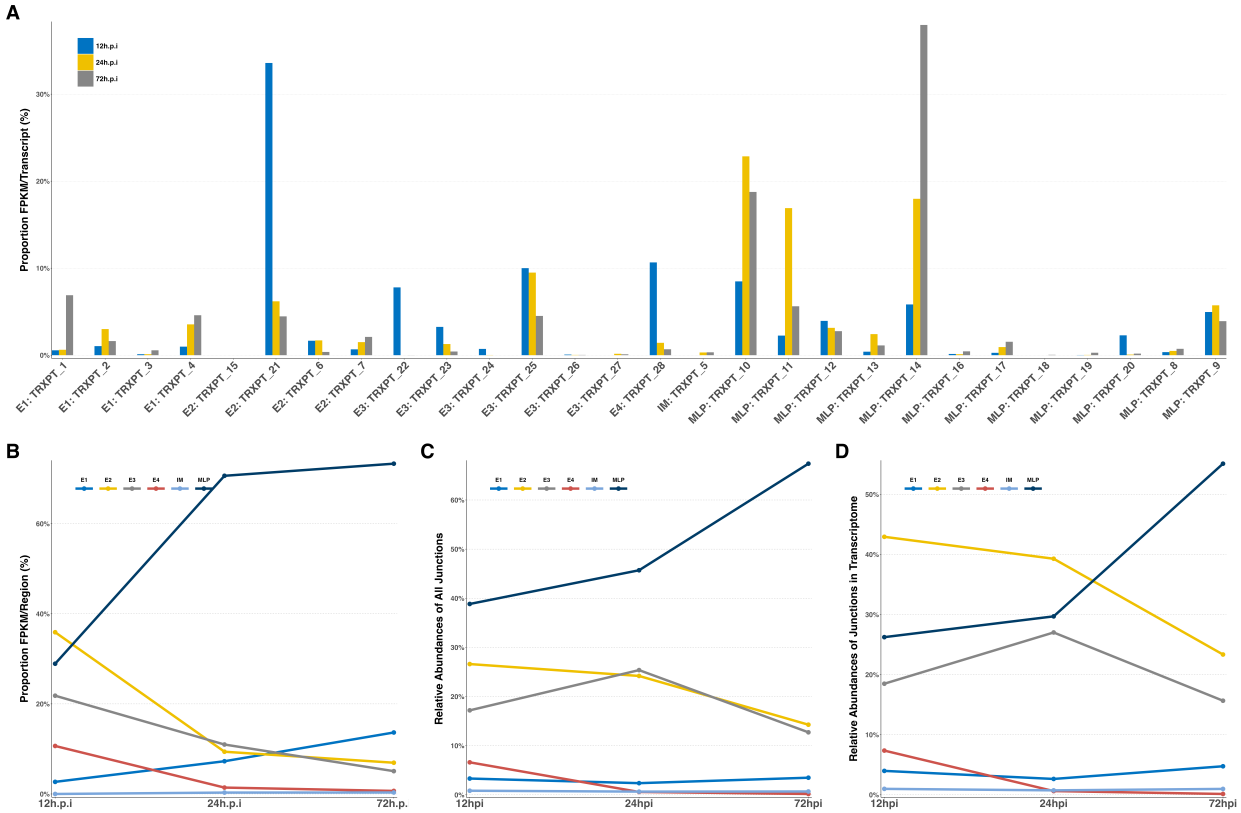

Figure 4: Changes in splicing and expression profile of THEV over time. a) *Normalized (FPKM) expression levels of transcripts over time*. The expression levels (FPKM) of individual transcripts as a percentage of the total expression of all transcripts at each time point are indicated. Only transcripts from our RNA-seq data are included here. **b)** *Normalized (FPKM) expression levels of transcripts by region over time*. The expression levels of each region/TU as a percentage of the total expression of all transcripts at each time point are indicated. Region expression levels were calculated by summing up the FPKMs of all transcripts categorized in that region. **c)** *Relative abundances of all splice junctions grouped by region/TU over time*. After assigning all **2,457** unique junctions to a TU and the total junction reads counted at each time point for each region, the total junction reads for each TU plotted as percentage of all junction reads at each time point is indicated. Note that the junction read counts are not normalized. **d)** *Relative abundances*

of junctions in transcriptome grouped by region/TU over time. This is identical to **(c)**, except that only the junctions found in the full transcriptome obtained from the RNA-seq data were included.

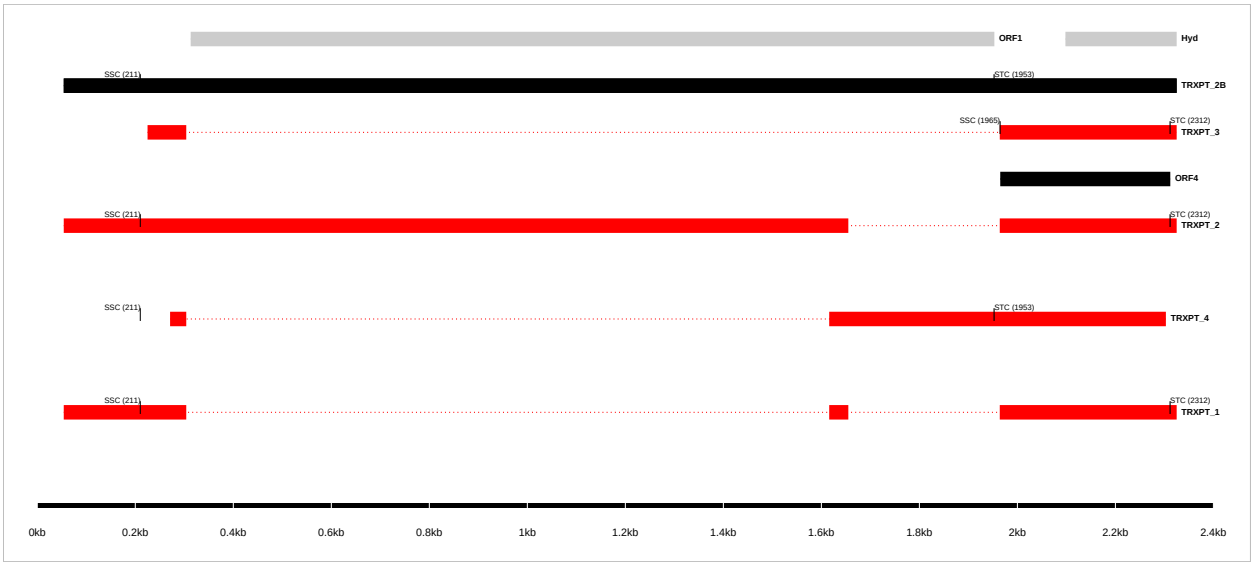

Transcript ID	Splice Junction				Strand	Junction Reads				Junction Status
	Start	End	Intron Length	Splice Donor−Acceptor		4h.p.i	12h.p.i	24h.p.i	72h.p.i	
TRXPT_1, TRXPT_4	304	1616	1313bp	GT−AG	+	0	9	1019	25041	Validated*
TRXPT_3	304	1964	1661bp	GT−AG	+	0	2	168	1588	Validated
TRXPT_2, TRXPT_1	1655	1964	310bp	GT−AG	+	0	9	1395	38491	Validated

*Not validated for TRXPT_4

Figure 5: The splice map of the E1 transcription unit (TU). Exons are depicted as boxes connected by introns (dotted lines). Transcripts from RNA-seq data are colored red, predicted ORFs are colored grey, and transcripts or ORFs discovered by other means are colored black. Each transcript or ORF is labelled with its name to the right. The start codon (SSC) and stop codon (STC) of the 5'-most CDS of each transcript is indicated with the nucleotide position in brackets. The region of the virus is depicted at the bottom as a black line with labels of the nucleotide positions for reference. The table shows sequence reads covering the splice junctions with information about their validation status using cloning and Sanger sequencing.

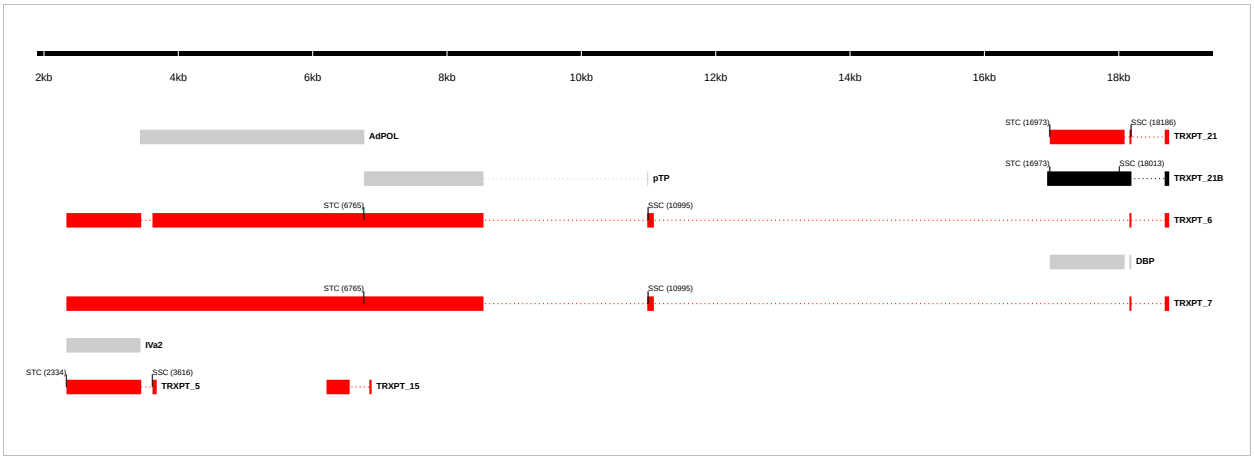

Transcript ID	Splice Junction Start	End	Splice Donor–Acceptor	Intron Length	Strand	region	Junction Reads 4h.p.i	12h.p.i	24h.p.i	72h.p.i	Junction Status
TRXPT_5, TRXPT_7	3447	3615	GT–AG	169bp	–	IM, E2	1	5	720	13422	Validated
TRXPT_6, TRXPT_7	11079	18159	GT–AG	7081bp	–	E2	0	2	0	0	Validated
TRXPT_21	18087	18159	GT–AG	73bp	–	E2	9	103	0	0	Validated
TRXPT_21, TRXPT_6, TRXPT_7	18189	18684	CT–AC, GT–AG	496bp	–	E2	0	111	18794	156037	Validated
TRXPT_6, TRXPT_7	8543	10981	GT–AG	2439bp	–	E2	0	0	298	850	Validated
TRXPT_15	6551	6843	GT–GC	293bp	–	E2	0	0	0	6	Validated

Figure 6: The splice map of the E2 and IM TUs. Exons are depicted as boxes connected by introns (dotted lines). Red transcripts are generated from RNA-seq data and predicted ORFs are colored grey. TRXPT_21B discovered by 3'RACE is colored black. Each transcript or ORF is labelled with its name to the right. The SSC and STC of the 5'-most CDS of each transcript is indicated with the nucleotide position in brackets. The region of the virus is depicted at the bottom as a black line with labels of the nucleotide positions for reference. The table shows sequence reads covering the splice junctions with information about their validation status using cloning and Sanger sequencing.

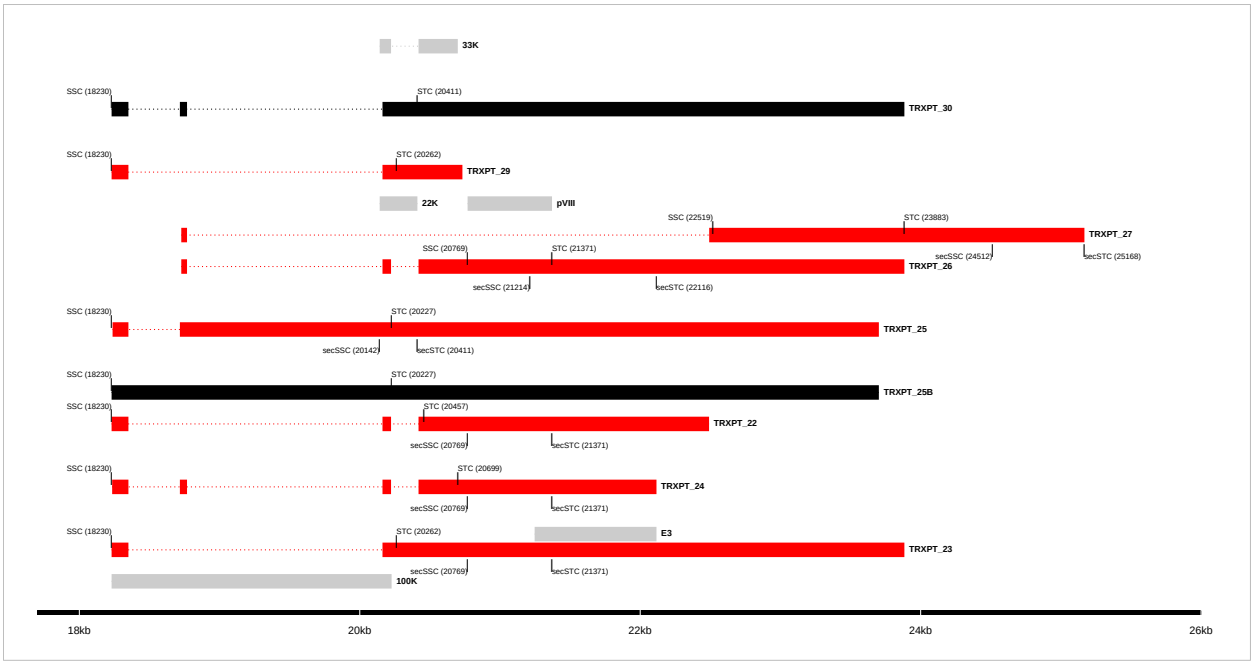

Transcript ID	Splice Junction				Strand	region	Junction Reads				Junction Status
	Start	End	Splice Donor–Acceptor	Intron Length			4h.p.i	12h.p.i	24h.p.i	72h.p.i	
TRXPT_25, TRXPT_24, TRXPT_10	18350	18717	GT–AG	368bp	+	E3, MLP	4	21	3930	35490	Validated
TRXPT_23, TRXPT_22, TRXPT_11	18350	20162	GT–AG	1813bp	+	E3, MLP	3	18	6619	38841	Validated
TRXPT_26, TRXPT_24, TRXPT_13, TRXPT_9, TRXPT_10	18768	20162	GT–AG	1395bp	+	E3, MLP	2	21	5207	45062	Validated
TRXPT_26, TRXPT_22, TRXPT_24, TRXPT_13, TRXPT_11, TRXPT_9, TRXPT_10	20223	20419	GT–AG	197bp	+	E3, MLP	3	33	10583	93238	Validated
TRXPT_27	18768	22492	GT–AG	3725bp	+	E3	0	0	101	1950	Validated

Figure 7: The splice map of the E3 TU. Exons are depicted as boxes connected by introns (dotted lines). Red transcripts are generated from RNA-seq data and predicted ORFs are colored grey. Transcripts discovered by other means are colored black. Each transcript or ORF is labelled with its name to the right. The start codon (SSC) and stop codon (STC) of the 5'-most CDS of each transcript is indicated with the nucleotide position in brackets. Similarly, the secondary SSC (secSSC) and secondary STC (secSTC) are shown. The region of the virus is depicted at the bottom as a black line with labels of the nucleotide positions for reference. The table shows sequence reads covering the splice junctions with information about their validation status using cloning and Sanger sequencing.

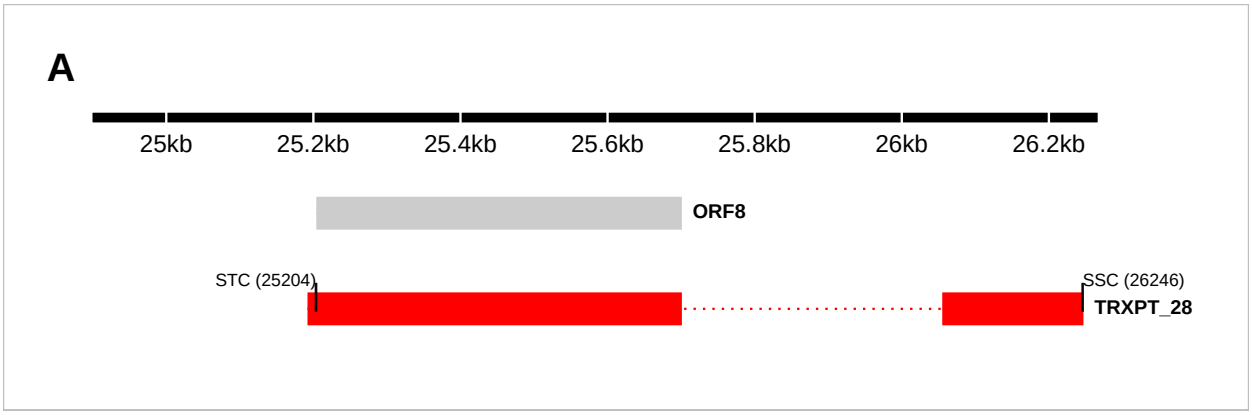

B

Transcript ID	Splice Junction Start	Splice Junction End	Splice Donor–Acceptor	Intron Length	Strand	Junction Reads 4h.p.i	Junction Reads 12h.p.i	Junction Reads 24h.p.i	Junction Reads 72h.p.i	Junction Status
TRXPT_28	25701	26055	GT–AG	355bp	–	1	37	602	1,894	Validated

Figure 8: The splice map of the E4 TU. Exons are depicted as boxes connected by introns (dotted lines). The transcript from RNA-seq data is colored red and the predicted ORF, grey. The transcript and ORF are labelled with their names to the right. The start codon (SSC) and stop codon (STC) of the 5'-most CDS is indicated with the nucleotide position in brackets. The region of the virus is depicted at the bottom as a black line with labels of the nucleotide positions for reference. The table shows sequence reads covering the splice junction with its validation status using cloning and Sanger sequencing.

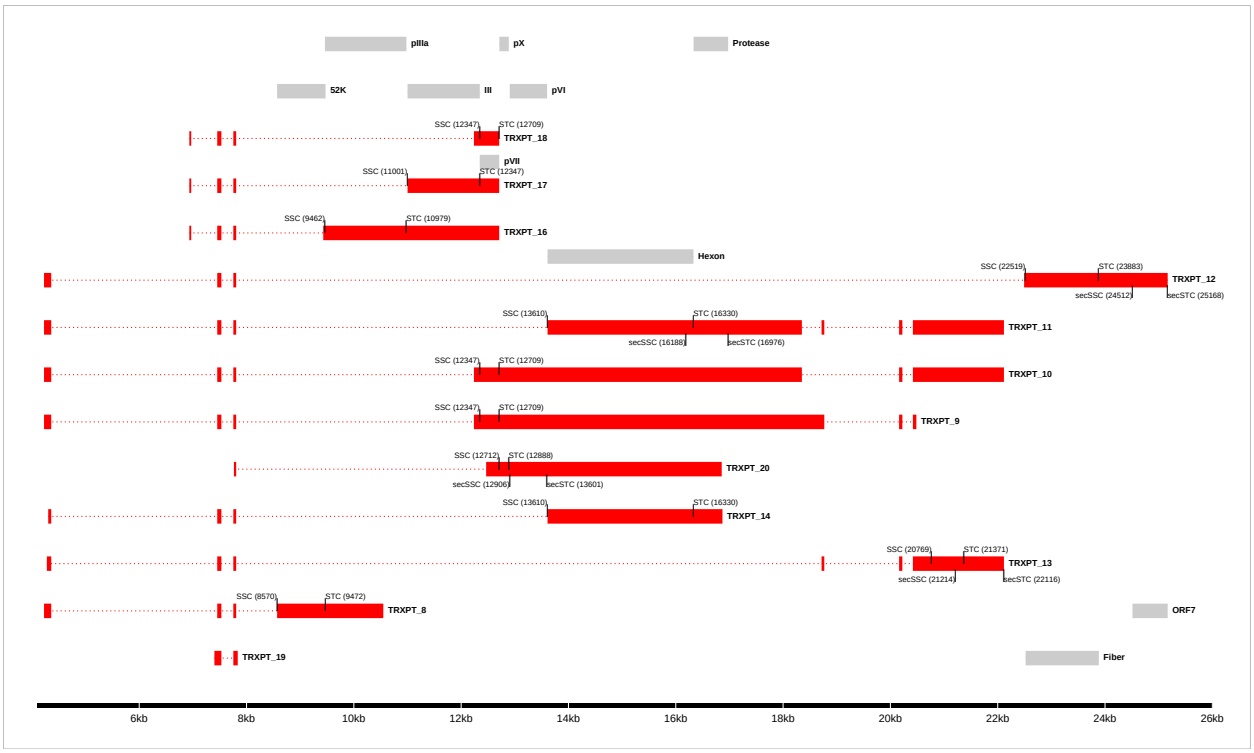

Transcript ID	Splice Junction					Junction Reads				
	Start	End	Splice Donor–Acceptor	Intron Length	Strand	4h.p.i	12h.p.i	24h.p.i	72h.p.i	Junction Status
TRXPT_13, TRXPT_8, TRXPT_14, TRXPT_10, TRXPT_12, TRXPT_11, TRXPT_9	4360	7454	GT–AG	3095bp	+	1	32	7128	179607	Validated
TRXPT_19, TRXPT_13, TRXPT_8, TRXPT_14, TRXPT_10, TRXPT_16, TRXPT_12, TRXPT_11, TRXPT_18, TRXPT_11, TRXPT_9	7531	7754	GT–AG	224bp	+	4	58	12319	322677	Validated
TRXPT_8	7807	8570	GT–AG	764bp	+	0	5	707	0	Validated
TRXPT_16	7807	11001	GT–AG	3195bp	+	0	1	226	10254	Validated
TRXPT_18, TRXPT_11, TRXPT_9	7807	12238	GT–AG	4432bp	+	0	7	2446	0	Validated
TRXPT_20	7807	12466	GT–AG	4660bp	+	0	3	437	0	Validated
TRXPT_14, TRXPT_10	7807	13610	GT–AG	5804bp	+	0	18	2553	0	Validated
TRXPT_13	7807	18717	GT–AG	10911bp	+	0	2	1391	0	Validated
TRXPT_12	7807	22492	GT–AG	14686bp	+	1	6	1642	21891	Validated
TRXPT_25, TRXPT_24, TRXPT_10	18350	18717	GT–AG	368bp	+	4	21	3930	35490	Validated
TRXPT_23, TRXPT_22, TRXPT_11	18350	20162	GT–AG	1813bp	+	3	18	6619	38841	Validated
TRXPT_26, TRXPT_24, TRXPT_13, TRXPT_9, TRXPT_10	18768	20162	GT–AG	1395bp	+	2	21	5207	45062	Validated
TRXPT_26, TRXPT_22, TRXPT_24, TRXPT_13, TRXPT_11, TRXPT_9, TRXPT_10	20223	20419	GT–AG	197bp	+	3	33	10583	93238	Validated
TRXPT_16, TRXPT_17, TRXPT_18	6969	7454	GT–AG	486bp	+	0	0	143	13482	Validated
TRXPT_17	7807	9430	GT–AG	1624bp	+	0	0	67	0	Validated

Figure 9: The splice map of the MLTU. Exons are depicted as boxes connected by introns (dotted lines). The transcripts from our RNA-seq data are colored red and the predicted ORFs, grey. The transcripts and ORFs are labelled with their names to the right. The start codon (SSC) and stop codon (STC) of the 5'-most CDS of each transcript is indicated with the nucleotide position in brackets. Similarly, the secondary SSC (secSSC) and secondary STC (secSTC) are shown. The region of the virus is depicted at the bottom as a black line with labels of the nucleotide positions for reference. The table shows sequence reads covering the splice junctions with information about their validation status using cloning and Sanger sequencing.

Table 1: Table 1: Overview of sequencing results

Metric	4h.p.i	12h.p.i	24h.p.i	72h.p.i	Total
Total reads	1.17e+08	7.63e+07	1.20e+08	1.15e+08	4.28e+08
Mapped (Host)	1.04e+08 (89.06%)	6.79e+07 (89.0393%)	1.06e+08 (88.2719%)	8.38e+07 (72.9802%)	3.62e+08
Mapped (THEV)	4.32e+02 (0.0004%)	6.70e+03 (0.0088%)	1.18e+06 (0.9841%)	1.69e+07 (14.6904%)	1.81e+07
Mean Per Base Coverage/Depth	2.42	37.71	6,666.96	95,041.7	101,749
Total unique splice junctions	13	37	236	2374	2,457
Junction coverage Total (at least 1 read)	37	605	115075	2132806	2.25e+06
Junction coverage Mean reads	2.8	16.4	487.6	898.4	351.3
Junction coverage (at least 10 reads)	0	13	132	1791	1,936
Junction coverage (at least 100 reads)	0	1	53	805	859
Junction coverage (at least 1000 reads)	0	0	18	168	186

Table 2: Table 2a: Most abundant splice junctions at 12h.p.i

Timepoint	Strand	Start	End	Splice_Site	Region	Intron Length	Reads (Percentage)
12hpi	-	18,087	18,159	GT-AG	E2	72 bp	103 (17%)
12hpi	+	18,189	18,684	CT-AC	MLP	495 bp	97 (16%)
12hpi	+	7,531	7,754	GT-AG	MLP	223 bp	58 (9.6%)
12hpi	-	25,701	26,055	GT-AG	E4	354 bp	37 (6.1%)
12hpi	+	20,223	20,419	GT-AG	E3	196 bp	33 (5.5%)
12hpi	+	4,360	7,454	GT-AG	MLP	3,094 bp	32 (5.3%)
12hpi	-	18,751	20,668	GT-AG	E2	1,917 bp	22 (3.6%)
12hpi	+	18,350	18,717	GT-AG	E3	367 bp	21 (3.5%)
12hpi	+	18,768	20,162	GT-AG	E3	1,394 bp	21 (3.5%)
12hpi	+	7,807	13,610	GT-AG	MLP	5,803 bp	18 (3%)
12hpi	+	18,350	20,162	GT-AG	E3	1,812 bp	18 (3%)
12hpi	-	18,189	18,684	GT-AG	E2	495 bp	14 (2.3%)
12hpi	-	18,751	21,682	GT-AG	E2	2,931 bp	10 (1.7%)
12hpi	+	304	1,616	GT-AG	E1	1,312 bp	9 (1.5%)
12hpi	+	1,655	1,964	GT-AG	E1	309 bp	9 (1.5%)
12hpi	-	18,087	18,163	GT-AG	E2	76 bp	8 (1.3%)
12hpi	+	7,807	12,238	GT-AG	MLP	4,431 bp	7 (1.2%)
12hpi	+	7,807	22,492	GT-AG	MLP	14,685 bp	6 (1%)

Table 3: Table 2b: Most abundant splice junctions at 24h.p.i

Timepoint	Strand	Start	End	Splice_Site	Region	Intron Length	Reads (Percentage)
24hpi	-	18,087	18,159	GT-AG	E2	72 bp	18,825 (16.4%)
24hpi	+	18,189	18,684	CT-AC	MLP	495 bp	17,670 (15.4%)
24hpi	+	7,531	7,754	GT-AG	MLP	223 bp	12,319 (10.7%)
24hpi	+	20,223	20,419	GT-AG	E3	196 bp	10,583 (9.2%)
24hpi	+	4,360	7,454	GT-AG	MLP	3,094 bp	7,128 (6.2%)
24hpi	+	18,350	20,162	GT-AG	E3	1,812 bp	6,619 (5.8%)
24hpi	+	18,768	20,162	GT-AG	E3	1,394 bp	5,207 (4.5%)
24hpi	+	18,350	18,717	GT-AG	E3	367 bp	3,930 (3.4%)
24hpi	-	18,751	20,668	GT-AG	E2	1,917 bp	3,870 (3.4%)
24hpi	+	7,807	13,610	GT-AG	MLP	5,803 bp	2,553 (2.2%)
24hpi	+	7,807	12,238	GT-AG	MLP	4,431 bp	2,446 (2.1%)
24hpi	+	7,807	22,492	GT-AG	MLP	14,685 bp	1,642 (1.4%)
24hpi	+	1,655	1,964	GT-AG	E1	309 bp	1,395 (1.2%)
24hpi	+	7,807	18,717	GT-AG	MLP	10,910 bp	1,391 (1.2%)
24hpi	-	18,189	18,684	GT-AG	E2	495 bp	1,124 (1%)
24hpi	-	18,751	21,128	GT-AG	E2	2,377 bp	1,124 (1%)
24hpi	+	20,223	20,894	GT-AG	E3	671 bp	1,208 (1%)

Table 4: Table 2c: Most abundant splice junctions at 72h.p.i

Timepoint	Strand	Start	End	Splice_Site	Region	Intron Length	Reads (Percentage)
72hpi	+	7,531	7,754	GT-AG	MLP	223 bp	322,677 (15.1%)
72hpi	+	4,360	7,454	GT-AG	MLP	3,094 bp	179,607 (8.4%)
72hpi	-	18,087	18,159	GT-AG	E2	72 bp	161,336 (7.6%)
72hpi	+	18,189	18,684	CT-AC	MLP	495 bp	146,425 (6.9%)
72hpi	+	20,223	20,419	GT-AG	E3	196 bp	93,238 (4.4%)
72hpi	+	7,807	13,610	GT-AG	MLP	5,803 bp	81,420 (3.8%)
72hpi	+	7,807	12,238	GT-AG	MLP	4,431 bp	77,616 (3.6%)
72hpi	+	18,768	20,162	GT-AG	E3	1,394 bp	45,062 (2.1%)
72hpi	+	1,655	1,964	GT-AG	E1	309 bp	38,491 (1.8%)
72hpi	+	18,350	20,162	GT-AG	E3	1,812 bp	38,841 (1.8%)
72hpi	+	18,350	18,717	GT-AG	E3	367 bp	35,490 (1.7%)
72hpi	+	304	1,616	GT-AG	E1	1,312 bp	25,041 (1.2%)
72hpi	-	18,751	20,668	GT-AG	E2	1,917 bp	26,338 (1.2%)
72hpi	+	7,807	12,904	GT-AG	MLP	5,097 bp	21,946 (1%)
72hpi	+	7,807	22,492	GT-AG	MLP	14,685 bp	21,891 (1%)